Journal of Electric Propulsion

RESEARCH Open Access

Laser-induced fluorescence spectroscopy on neutrals for plasma studies in Hall thrusters

Matteo Da Valle[1*], Yordanka Dancheva[2], Alen Khanbekyan[1], Pietro Coniglio[2], Emilio Mariotti[1,3] and Fabrizio Scortecci[2]

*Correspondence:
m.davalle@student.unisi.it

[1] DSFTA, University of Siena, via Roma 56, Siena 53100, SI, Italy
[2] Aerospazio Tecnologie S.r.l., via dei Tessili 99, Rapolano Terme 53040, SI, Italy
[3] INFN - sez. Pisa, Largo B. Pontecorvo 3, Pisa 56127, PI, Italy

Abstract

Hall thrusters offer an excellent balance between specific impulse and thrust-to-area ratios. However, adapting them to new power requirements is challenging because of the complexity of plasma dynamics and material interactions. This study focuses on using a minimally intrusive diagnostic tool, laser-induced fluorescence (LIF) spectroscopy, to investigate the atomic population within an electric thruster. We developed a comprehensive LIF spectra simulator incorporating factors such as the natural gas mixture and the Doppler Effect. By leveraging the anomalous Zeeman Effect, we achieved accurate non-intrusive measurements of the local magnetic field vector, a critical parameter for the thruster design process. We propose a new data elaboration strategy that combines measurements taken with two orthogonal laser polarizations inside the vacuum chambers. This strategy was successful in decoupling the neutrals' temperature and magnetic field values inferred from LIF spectra. An experimental campaign within a laboratory model Hall thruster operating with Krypton validated this approach and demonstrated the technique's potential. Three different LIF excitation schemes were used, with small discrepancies in the inferred values of the model variables. The transitions starting from the level $5s'\left[1/2\right]_1$ led to the best precision in the evaluation of the neutrals' temperature and the local magnetic field. The neutrals' drift velocity experiences an apparent acceleration until the exit of the thruster channel, which could be due to charge-exchange collisions or slow neutrals' population depletion caused by ionization.

Keywords: LIF, Laser-induced fluorescence, Hall thruster, Zeeman Effect, Magnetic field, Neutrals

Introduction

Hall thrusters are advanced electric propulsion systems able to offer a great compromise between specific impulse and thrust-to-area ratio [1, 2]. Scaling laws offer a strong tool in adapting a previously optimized thruster to new power requirements [3, 4], but their use is limited mostly to a first design. Despite advancements in numerical simulations, capturing all the complexities of plasma dynamics and material interactions remains challenging [2, 5], making them difficult to use for the thruster optimization and qualification phases. As a result, diagnostic tools become crucial for deeply understanding the thruster operation and capabilities or even to validate numerical simulators. Between

the several tools, non-intrusive diagnostics are increasing in popularity, showing good capabilities in witnessing plasma instabilities and parameters without modifying the thruster working principle [6–8].

In this work, the focus will be given to a specific minimally intrusive laser spectroscopy technique, laser-induced fluorescence (LIF) spectroscopy. It works by illuminating the plasma with a laser, finely tuned around a specific frequency that matches a resonant transition of one of the species in the plasma. The resulting fluorescence is then collected, from which various important plasma parameters can be recovered. Thanks to its species-selective nature, neutral and ion populations of different atoms can be individually investigated. Many articles show its capabilities of measuring ion's velocity distribution function (IVDF) with great spatial resolution [7, 9]. Ref. [10] shows a way of recovering some of the most critical parameters from LIF measurements, such as electric field and ionization frequency. This was possible only thanks to an elaboration of the spatially resolved IVDF. Moreover, in Refs. [11–14] LIF was used to reconstruct the time-resolved IVDF, opening this tool to the analysis of plasma oscillations inside the thrusters, hence, strongly enhancing the potential of the diagnostic.

Using LIF on neutrals may seem less significant, as they have negligible interaction with the electromagnetic field. However, neutral LIF spectra can potentially contain information about the *in situ* magnetic field. This is achieved by leveraging the Zeeman Effect, which alters the LIF spectra and has a more noticeable impact on neutrals due to their narrower VDF. Consequently, this enables the non-intrusive magnetic field measurement during thruster operation within the channel itself, one of the most critical parameters during the design phase for the management of collision frequency and erosion processes [5]. Applications of this technique in Hall thrusters can be traced back to Refs. [15, 16], which provided the first set of measurements of the local magnetic field with a non-intrusive method. Differently, Ref. [17] focused on the neutral population flow properties, showing an increment of the drift velocity throughout the thruster channel and highlighting the primary causes of that phenomenon. Finally, in a more recent work, the technique was applied on a Helicon plasma thruster, leveraging the prior knowledge of the geometry of the magnetic field to extract accurate information on the atomic population [18].

This study explores the extraction of information from neutral LIF, including neutral drift velocity and local magnetic field, without assumptions about its direction. We conducted an experimental campaign using a laboratory model Hall thruster that uses Krypton as the propellant to validate the technique and evaluate its capabilities. The choice of the propellant was made because thanks to its more cost-effective nature, the space industry is slowly replacing Xenon with Krypton, for which fewer studies are available in the literature.

In "Experimental setup" section, we present the experimental setup used during the campaign. "Lineshape modeling" section is dedicated to the LIF spectra model. Starting from a brief background on the generic lineshape, the final data fit model and methodology are deduced by introducing the necessary hypothesis on the geometry of the laser-atom interaction. Special attention is given to the Zeeman Effect, modelled here with no assumptions on magnetic field orientation or laser polarization state. Finally, in "Experimental campaign results" section the measurement strategy and the experimental

campaign results are shown. Considerations regarding the main fit parameters from these results are given, to witness the strength of the technique and its potential for improving existing Hall thrusters or for the design of innovative plasma thrusters.

Experimental setup

Hall thruster

The Krypton LIF measurements presented in this work were made in one of the facilities of Aerospazio Tecnologie S.r.l. in Rapolano Terme. The laboratory model HET (see Fig. 1) fired Krypton in a non-magnetic stainless steel vacuum chamber with a base pressure as low as 10^{-7} mbar, increasing to a range of 2×10^{-5} mbar to 5×10^{-5} mbar (Kr equivalent) during the thruster operation.

The thruster anode voltage V_A was set to 250 V, with a discharge current I_D of 0.65 A, for a power of about 160 W. A central coil generates the static and mostly radial magnetic field. Its current is modified to have the ExB discharge and to scale, at least in a first approximation, the magnetic field intensity to validate the magnetic field measurements. A maximum discharge current oscillation of 50 mA_{rms}, comprehensive of longitudinal modes and probe white noise, was measured during operation, assuring a stable channel discharge with negligible oscillations in the plasma parameters. The thruster was mounted on two orthogonal translation stages, employed to modify its position with respect to the LIF measurement point in the horizontal plane, thus enabling the analysis in multiple spatial points (see Fig. 3).

Optical setup

A Fabry-Perot diode laser emitting around 830 nm is used as laser source. With a proper combination of diode temperature and current, we were able to analyze three different Kr I resonant transitions, of which the LIF excitation-fluorescence schemes are shown in Fig. 2.

After passing through a Faraday isolator to protect the diode, the beam polarization is adjusted and analyzed with a combination of a fiber paddle, a polarization beam splitter

Fig. 1 Laboratory model Hall thruster during operation with Krypton

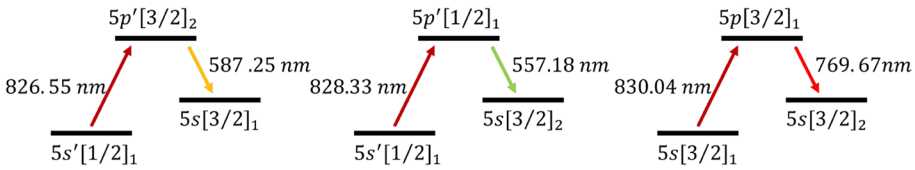

Fig. 2 Kr I LIF excitation-fluorescence schemes used for the experimental campaign. Racah notation is used to define the electronic states

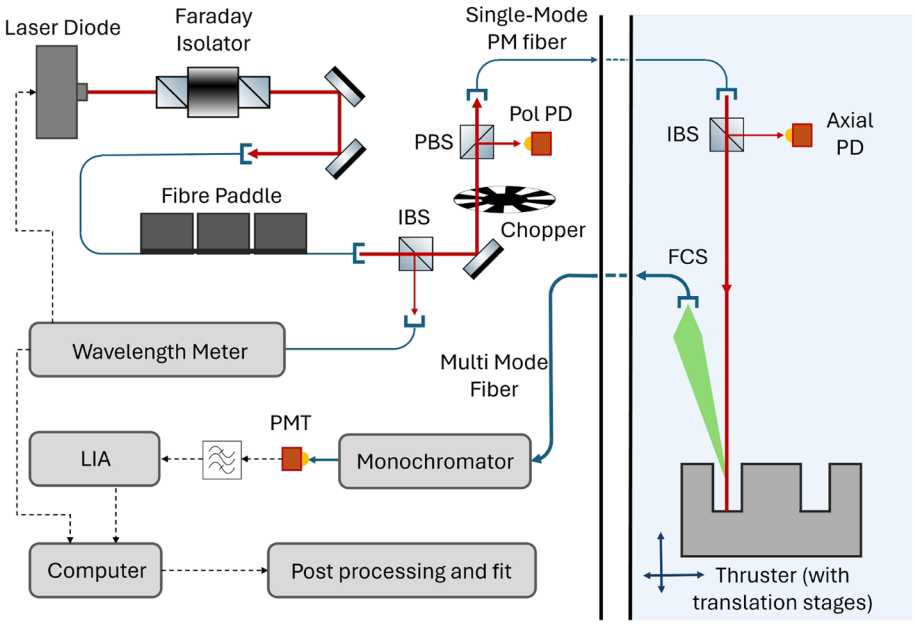

Fig. 3 LIF experimental setup. The light blue background corresponds to the inside of the vacuum chamber. The red line is the laser beam; the blue lines are the various optical fibers used in the setup; the black segmented lines are the electric connections

(PBS) and a photodiode (Pol PD on Fig. 3). Hence, the linearly polarized beam is coupled along the slow or fast axis of a single-mode polarization-maintaining fiber (PM fiber). These fibers decouple the polarization state in the two aforementioned axes by intentionally introducing a systematic linear birefringence [19]. Ultimately, when the polarization is perfectly aligned with the slow or fast axis, it will remain unchanged at the fiber exit. A small angle α between the PBS axis and the PM fiber axes will result in a small ellipticity with an indefinite phase shift ε. In our setup, we estimated α to be less than 5° and included this misalignment in the data fit model (see "Lineshape modeling" section).

Two intensity beam splitters (IBS) are used to direct the laser beam for wavelength and intensity measurements. The first takes a small beam fraction to a high-accuracy (± 10 MHz) wavelength meter. Therefore, utilizing a feedback control system, the wavelength meter modifies the laser diode current, adjusting the laser wavelength to scan around the three transitions. With this control, several GHz can be scanned without incurring into mode hops. The second intensity beam splitter, positioned inside the chamber, redirects a small portion of the beam to a photo-diode in the vacuum chamber (Axial PD), previously calibrated to compute the laser intensity right before interacting with the plasma.

The fluorescence collection system (FCS) consists of an ad-hoc optical system focusing on 600 μm multi-mode fiber the fluorescence coming from a small cone. Therefore, the small volume resulting from the intersection of the laser beam in the chamber and the FCS field-of-view corresponds to the LIF measurement point. The intersection point has an elliptic shape of about 1 mm x 1.4 mm.

The collected fluorescence is then filtered by a monochromator and converted to an analogue signal through a photomultiplier. Finally, we use a lock-in amplifier (LIA) to discriminate the previously modulated signal from the unwanted noise. The intensity modulation was generated by utilizing an optical chopper on the beam which operates at about 290 Hz.

A schematic of the setup is shown in Fig. 3. A more complete description of the experimental apparatus can be found in Refs. [7, 20].

Lineshape modeling

The laser-induced fluorescence spectra contain information regarding the small fraction of the interrogated plasma. Many effects can modify their shapes, and analyzing how these effects influence the spectra can help reconstruct parameters such as magnetic field intensity or population temperature. Therefore, the model of the interaction between the plasma and the laser should account for every phenomenon with a non-negligible impact on the resulting fluorescence spectrum.

In the model proposed, the Doppler Effect, natural broadening, hyperfine structure and isotopic shifts are considered [21, 22]. A particular focus is given to the anomalous Zeeman Effect resulting from the interaction between the magnetic field $\vec{B}$ and the atomic angular momenta. This will make it possible to have a local measure, during the thruster operations, of one of the most important parameters for Hall thrusters, the magnetic field.

In general, the fluorescence spectrum can be modelled as a convolution product of three functions:

$$I(\nu) \propto (G * l * h)(\nu) \tag{1}$$

Here $G(\nu(\upsilon))$ derives from the Doppler Effect only and, if recovered, can give the normalized 1D velocity distribution function (VDF) along the laser direction. In our study, we assumed G with a Maxwell-Boltzmann VDF with undefined mean velocity υ_N and temperature T, an assumption that fits well with the data taken inside the thruster channel. l is a Lorentzian function that includes transition lifetime and possible transition saturation effects. Finally, h consists of a summation of Dirac deltas $\sum_i k_i \sum_j a_{ij}\delta(\nu - \nu_{ij})$ that includes isotopic shifts and abundances, the anomalous Zeeman Effect and, when present, the hyperfine structure; $\nu_{ij}(\vec{B})$ and $a_{ij}(\vec{B})$ are the j^{th} transition resonance frequency and transition intensity for the i^{th} isotope, of which the relative abundance is k_i.

The anomalous Zeeman Effect

By temporarily neglecting the potential hyperfine structure arising from nuclear spin I, the anomalous Zeeman Effect can be considered as a perturbation of the fine structure. This assumption enormously simplifies its modelling since the fine structure total angular momentum quantum number J and its projection on the quantization axis m_J remain

good quantum numbers. From the usual selection rules for electric dipole transitions, only transitions in which $|m_{Ju} - m_{Jl}| \leq 1$ are allowed. The Zeeman Effect removes the degeneracy in the m_J levels with the same J quantum number.

Therefore, transitions will be shifted by:

$$h(\nu_{ij}(B) - \nu_{ij}(0)) = (g_{Ju} m_{Ju} - g_{Jl} m_{Jl}) \mu_B B \tag{2}$$

with a shift proportional to B and depending on the Landé factors g_J and the quantum numbers m_J of both the upper ($_u$) and lower ($_l$) states. With a circularly polarized laser beam in the magnetic field reference frame, only transitions with $m_{Ju} - m_{Jl} = \pm 1$ are allowed, respectively σ^+ and σ^- transitions. Instead, if the polarization is aligned with the magnetic field, only transitions with $m_{Ju} = m_{Jl}$ arise (π transitions).

In a more general case, a combination of the three transitions will be present in the fluorescence spectrum, and their intensities will be proportional to the coordinates resulting from the decomposition of the polarization vector in a spherical basis in the $\vec{B}$ frame. We use Wigner 3-j symbols to compute the single transition intensities a_{ij} [21, 23], which are then scaled with the corresponding total normalized intensity resulting from the decomposition.

Having Fig. 4 as reference for the geometrical angles θ and ϕ and "Experimental setup" section for the beam polarization angles α and ε, the scaling factors for the three kinds of transitions are:

$$\begin{aligned} I_\pi &= \sin(\theta)^2(\cos(\phi - \alpha)^2 - \sin(2\alpha)\sin(2\phi)\sin(\varepsilon/2)^2) \\ I_{\sigma^\pm} &= (1 - I_\pi \pm \cos(\theta)\sin(2\alpha)\sin(\varepsilon))/2 \end{aligned} \tag{3}$$

Therefore, π and $\sigma^\pm$ transitions will have different scaling coefficients depending on the magnetic field orientation. Consequently, with the knowledge of the laser beam polarization state, a full reconstruction of the local $\vec{B}$ can be done by analyzing the LIF spectrum.

In the presence of hyperfine splittings ($I \neq 0$), a more advanced procedure must be done to compute ν_{ij} and a_{ij}. In our case, the Zeeman Effect and the hyperfine interaction may have comparable order of magnitude in how they perturb the atom, but they still have a negligible impact w.r.t. the fine interaction. Therefore, we treat the two perturbing effects at the same level and the right quantum numbers for the analysis are the fine interaction numbers J and m_J together with the nuclear interaction numbers I and m_I.

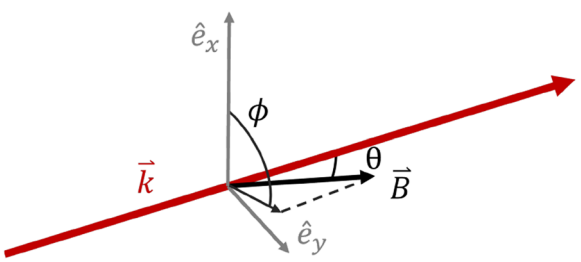

Fig. 4 Definition of geometrical angles θ and ϕ in the spherical coordinates system aligned with the laser vector $\vec{k}$

At the same time, the Zeeman Effect can be analyzed starting from an already perturbed atomic state from the hyperfine interaction. Hence, the Hamiltonian $\mathcal{H}$ of the interaction can be written as the sum of the Hamiltonian $\mathcal{H}_0$, which includes only the hyperfine interaction, and the Zeeman Hamiltonian:

$$\mathcal{H} = \mathcal{H}_0 - \left(\frac{\mu_B}{\hbar}\right)\mathbf{B}\cdot(g_J\mathbf{J} + g_I\mathbf{I}) \tag{4}$$

$\mathcal{H}_0$ is a diagonal matrix that can be computed with the knowledge of the hyperfine structure constants [21], whereas the Zeeman Hamiltonian presents non-diagonal terms too. Therefore, we perform a diagonalization of $\mathcal{H}$ from which eigenvalues and eigenvectors are recovered. The first ones give the energy level shifts w.r.t. the fine structure resonance $h(\nu_{ij}(B) - \nu_{ij}(0))$. The eigenvectors are used to define the new state vectors $|\psi(F, m_F)>$ as functions of the hyperfine interaction state vectors $|F, m_F>$:

$$|\psi(F, m_F)> = \sum_{F'} C_{F'F}|F', m'_F> \tag{5}$$

F and m_F are the hyperfine interaction quantum numbers. It is important to notice that the new state vectors are a linear combination of the old hyperfine state vectors since F and m_F are not valid quantum numbers after the Zeeman Effect perturbation. Finally, we use the eigenvectors $C_{F'F}$ for the computation of $a_{ij}(\vec{B})$, starting from $a_{ij}(0)$ which can be calculated by using Wigner 3-j and 6-j symbols. This procedure, to compute the spectra in the presence of both hyperfine structure and Zeeman Effect, can be found in Ref. [24], including the full mathematical procedure and the experimental validation.

Kr I transitions

We considered three different Kr I LIF excitation schemes to interrogate the neutral Kr (see Fig. 2). The selection took into consideration several reasons, such as the previous knowledge of the various parameters, the presence of a high excitation cross section (e^- + Kr) to have a good starting level number density [25] and, obviously, the capabilities of our optical system (see "Experimental setup" section). Table 1 summarizes some of the main parameters needed for the simulation of each transition [26, 27] and Fig. 5 shows the various resonances that compose the total spectra with $B = 0$.

Only one of the six stable isotopes, ^{83}Kr, has a nuclear spin of $I = 9/2$. Therefore, only this isotope requires the diagonalization of the Hamiltonian $\mathcal{H}$. On the contrary, Eq. 2 is extremely accurate for all the other stable isotopes, significantly reducing the computational time. We use the Faddeeva function $w(z) = exp(-z^2)erfc(-iz)$ to compute the convolution of the Gaussian profile G with the Lorentzian function l.

Table 1 Kr I excitation schemes selected for LIF diagnostic

Excited transition	λ (nm)	g_{Ju}	g_{Jl}	Detected transition	λ (nm)
$5s'[1/2]_1 \rightarrow 5p'[3/2]_2$	826.55140	1.259	1.1819	$5p'[3/2]_2 \rightarrow 5s[3/2]_1$	587.254320
$5s'[1/2]_1 \rightarrow 5p'[1/2]_1$	828.33284	1.259	1.451	$5p'[1/2]_1 \rightarrow 5s[3/2]_2$	557.183623
$5s[3/2]_1 \rightarrow 5p[3/2]_1$	830.03907	1.2428	1.0096	$5p[3/2]_1 \rightarrow 5s[3/2]_2$	769.66579

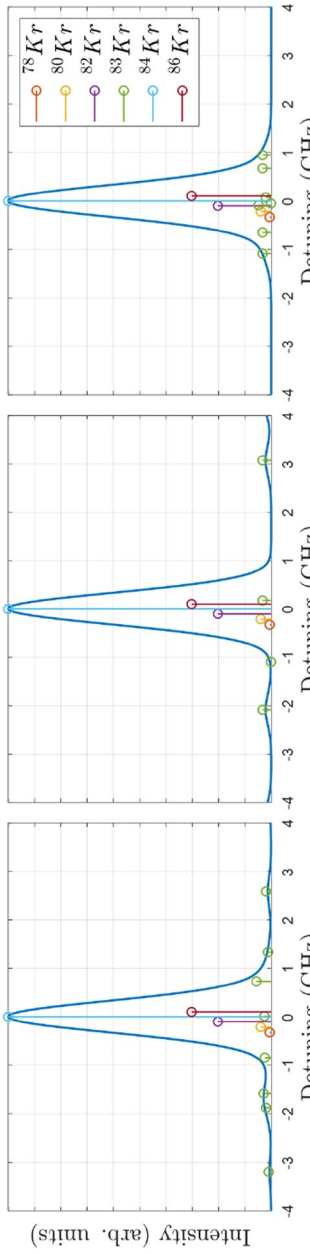

Fig. 5 Kr I transitions spectra in the absence of magnetic field. From the left, excitation at 826.55 nm, 828.33 nm and 830.04 nm, respectively. The blue line is the total spectrum computed with $T = 700$ K

Figure 6 shows an application of the model described in the previous subsections for the three spectra, considering the saturation effect negligible. Since $g_{Ju} \approx g_{Jl}$ for all three transitions, minimal variations between the cases with only π transitions and those at $B = 0$ are visible (see Eq. 2). On the contrary, the combination of σ^+ and σ^- transitions is the one that modifies the most the LIF spectra, since in these cases we have $m_{Ju} - m_{Jl} = \pm 1$.

Data elaboration

Bayesian approach

To extract the plasma parameters from LIF measurements, we used a Bayesian statistical approach. The Bayesian statistic uses previous knowledge of some model parameters to increase fit capabilities. This information is contained in the prior distribution $p_I(\mathbf{\Theta}|\mathrm{M})$, where $\mathbf{\Theta}$ consists of all the variables in the model such as B or T. Therefore, the calculation of the probability distribution on the model variables called the posterior distribution $p_D(\mathbf{\Theta}|data, \mathrm{M})$, is:

$$p_D(\mathbf{\Theta}|data, \mathrm{M}) = \frac{\mathrm{L(data}|\mathbf{\Theta}, \mathrm{M)p_I}(\mathbf{\Theta}|\mathrm{M})}{\mathrm{p_E(data}|\mathrm{M})} \tag{6}$$

$L(data|\mathbf{\Theta}, \mathrm{M})$ represents the likelihood, assumed as a multivariate normal distribution without correlation between the data. This assumption is justified since only white noise remains after an ad hoc under-sampling of the collected data to match the LIA bandwidth. Finally, $p_E(data|\mathrm{M})$ is the evidence used to normalize the numerator to finally have a probability distribution function.

The computation of the posterior from Eq. 6 can be computationally heavy. Therefore, we used an MCMC (Markov-Chain Monte Carlo) based algorithm for the task with already proven capabilities [28–31]. From the posterior distribution, multiple pieces of information are extracted such as the most probable value and credible intervals for each variable. The credible intervals are computed following the principle of highest posterior density interval, therefore taking the narrower interval around the mode, for which the integral of the marginalized $p_D(\mathbf{\Theta}|data, \mathrm{M})$ satisfies the credibility requirement.

Furthermore, correlation analyzes are performed to help understand the strengths and weaknesses of the fitting methodology used and eventually improve it, as will become clear in the following sections.

Measurement strategy for the experimental campaign

Proposed methodology

Different strategies can be adopted. Usually, the chosen one consists of maximizing the intensity of the σ^+ and σ^- transitions, to increase the dependence of the fluorescence spectrum on $\vec{B}$ (Eq. 2). Looking at Eq. 3, two possibilities can lead to that outcome: $\theta = 0°$ or $\phi - \alpha = 90°$. In the first case, the laser beam should be aligned with $\vec{B}$ [18], and in the second case, the beam polarization must be orthogonal to $\vec{B}$ [15]. Using Eq. 3, the spherical basis decomposition would lead to:

$$I_\pi = 0 \quad I_{\sigma^\pm} = 1/2 \tag{7}$$

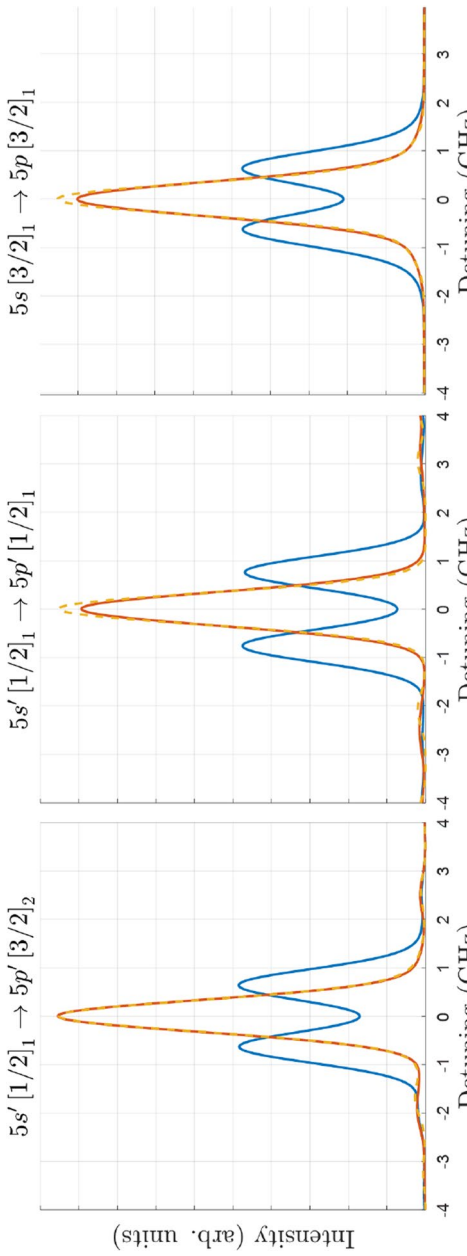

Fig. 6 Kr I transitions in the presence of magnetic field. From left, respectively, 826.55 nm, 828.33 nm and 830.04 nm. All spectra are computed with $T = 700$ K. The segmented yellow lines are the spectra without B; the blue lines with equal combinations of σ^+ and σ^- transitions ($I_{\sigma^+} = I_{\sigma^-} = 0.5$); the orange lines with only π transitions ($I_\pi = 1$). The magnetic field intensity used in the simulations is $B = 400$ G

Therefore, by knowing the magnetic field direction, it could be possible to create an ad hoc optical setup that can polarize the beam in this manner. Unfortunately, in some thrusters, self-induced $\vec{B}$ can significantly influence the global $\vec{B}$ [32]. Therefore, assuming that the magnetic field direction does not change during the thruster operation can lead to inaccuracies. Furthermore, since a spectrum made of π transitions ($m_{Ju} = m_{Jl}$) is almost unaffected by the magnetic field, it could be useful to measure neutrals' temperature and drift velocity, without the significant influence from the Zeeman Effect.

The strategy we propose takes advantage of the possibility of rotating the polarization in two orthogonal directions in our experimental apparatus (see "Experimental setup" section). It consists of taking two measures of the LIF spectrum for each position, one with horizontal polarization ($\alpha \approx 0°$) and the other with vertical polarization ($\alpha \approx 90°$). This strategy would permit measuring with good precision many different magnetic field geometric configurations, making the diagnostic system more robust and significantly reducing the correlation between T and B.

Data fitting model

The generic lineshape model defined in "Lineshape modeling" section does not impose any constraints on either the experimental setup or the thruster magnetic field. Two possibilities can arise:

- the laser beam is aligned with the PM fiber slow axis. Hence, $\alpha = 0° \pm 5°$. We will refer to this configuration as horizontal H;
- the laser beam is aligned with the PM fiber fast axis. Hence, $\alpha = 90° \pm 5°$. We will refer to this configuration as vertical V.

Furthermore, since the campaign measurements are made in the thruster channel center-line, we can assume a quasi-radial magnetic field vector $\vec{B}$, with $\theta \to 90°$ and $\phi \to 0°$, even when inserting the self-induced magnetic field. Starting from Eq. 3 and introducing these considerations, we reduced the data fitting model to:

$$\mathrm{H}: \begin{cases} I_\pi^H \approx \sin(\theta)^2 \cos(\phi - \alpha)^2 = \sin(\theta^*)^2 \\ I_{\sigma^\pm}^H \approx \left[1 - \sin(\theta^*)^2\right]/2 \end{cases} \quad \mathrm{V}: \begin{cases} I_\pi^V \approx 0 \\ I_{\sigma^\pm}^V \approx 1/2 \pm \delta \end{cases} \quad |\delta| < 0.10 \tag{8}$$

Here we introduced two new variables used in the fit: θ^* and δ. The first one is a fictitious angle containing information of both θ and ϕ. This angle is expected to be close to 90° from geometrical constraints. δ accounts for possible ellipticity in the beam, which would introduce a difference in the two σ transition intensities, negligible for the horizontal case. Since $|\delta| \leq sin(2\alpha)/2$ ($\delta = cos(\theta)sin(2\alpha)sin(\varepsilon)/2$, Eq. 3), from previous precision considerations made on α, a maximum value of 0.1 is expected.

Therefore, the model variables are reduced to seven:

- θ^* and $|\delta|$ as geometrical parameters;
- B, the magnetic field intensity, which defines the frequency shifts through Eq. 2;
- the neutrals' temperature T and drift velocity υ_N, contained inside G, having assumed an MB distribution function for the neutrals' velocity;

- two intensity scaling factors, one for the horizontal configuration and one for the vertical one.

Experimental campaign results

Multiple goals were considered during the campaign:

1. validation of the theoretical model and the data elaboration strategy;
2. analysis with LIF of the Kr atoms flow inside the channel. Therefore, the experimental determination of the magnetic field vector and the evolution of the atoms' flow parameters, but also the comparison of the fit capabilities with different excitation-fluorescence schemes;
3. evaluation of the strengths and weaknesses of our setup, to further improve it and increase its performance.

Every measure consisted of a 12 pm wavelength scan around the resonant frequency, lasting 150 seconds, for each polarization configuration. Multiple scans were overlapped to increase the signal-to-noise ratio (SNR), mostly close to the channel exit. The intensity of the laser was around 2 mW/mm^2, a value for which saturation effects were estimated to be small.

Theoretical model and strategy validation

Residual analysis

The common and most effective way to validate a model is by examining the residuals in the fit. Two examples of residual analysis are shown in Fig. 7. These examples were taken 2 mm and 6 mm upstream of the channel exit by exploiting the $5s'[1/2]_1 \rightarrow 5p'[1/2]_1$ transition (see Table 1).

A small trend different from white noise can be seen near the tails of the spectra. Between the various reasons, we identify as the main suspect for these tiny discrepancies a small, yet present, broadening due to the Lorentzian function l, which may be caused by transition saturation or by collisional broadening mechanisms. Another possibility could reside in the assumption of a perfect MB velocity distribution function of the neutrals. Nevertheless, the fit was still extremely accurate and, therefore, the model behaved according to our expectations.

B/I_C ratio validation

A second validation test was made by taking several measurements in the same thruster location and with different magnetic field intensities, assuming a linear relationship between the coil's current I_C and the magnetic field generated.

Figure 8 shows the most probable value and credibility interval for the magnetic field intensity B and direction θ for different I_C. These measurements were taken in the channel center-line, 4 mm upstream of the channel exit, with a reference I_C of 0.4 A. The $5s'[1/2]_1 \rightarrow 5p'[1/2]_1$ transition (see Table 1) was used for this analysis.

Even if every measure consisted of only one scan lasting 150 seconds, the model was still able to measure a constant B/I_C ratio with really good accuracy, validating the theoretical model. For θ^* similar considerations can be done even though only an upper limit

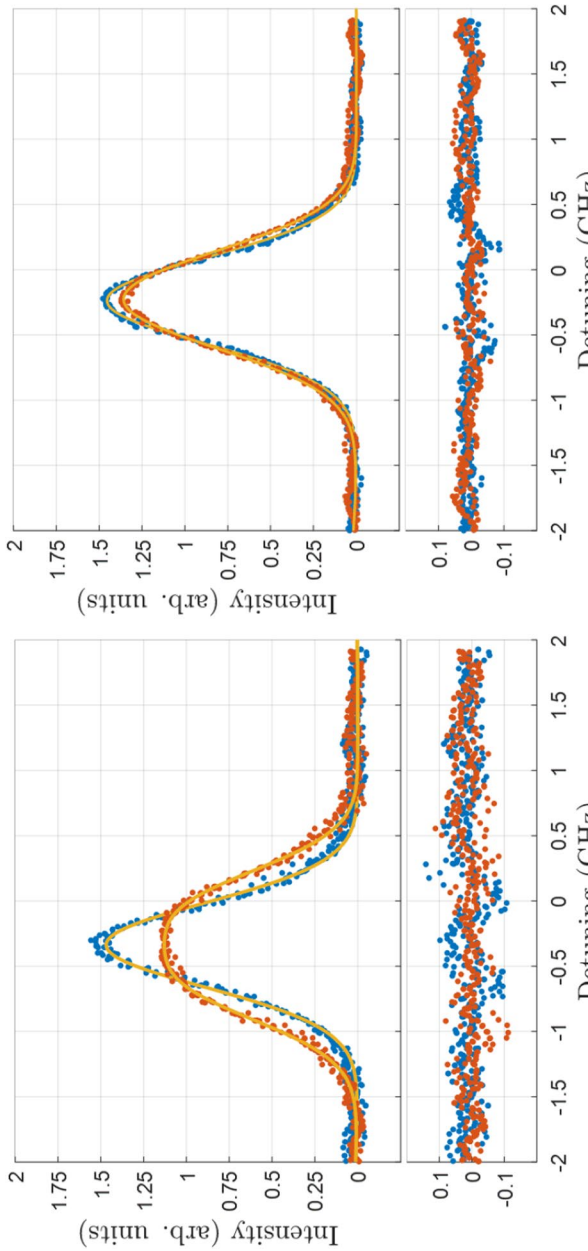

Fig. 7 Residual analysis for intermediate and low magnetic field intensities. The yellow line represents the best fit with our model; blue dots are measured data with horizontal polarization; red dots are measured data with vertical polarization. The bottom plots show the residuals

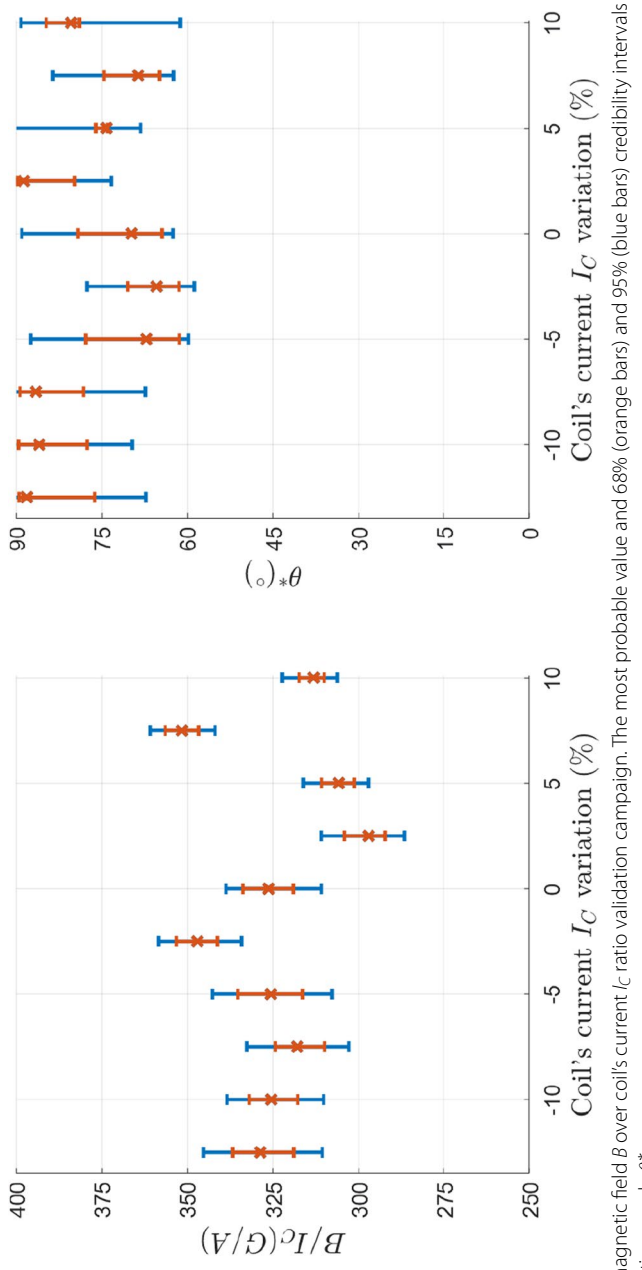

Fig. 8 Results of the magnetic field *B* over coil's current I_C ratio validation campaign. The most probable value and 68% (orange bars) and 95% (blue bars) credibility intervals are shown for the fitted ratio and the fictitious angle θ^*

is deduced, and, therefore, a higher signal-to-noise ratio would be needed to infer the precise value. Small differences in the measured magnetic field could derive from a different self-induced $\vec{B}$, since by modifying the coil's current we are also slightly modifying the ionization and acceleration processes. Instead, the discrepancies observed in the coil's current variations of -2.5% and above $+7.5\%$ may result from the thruster's unstable behavior during those measurements. This instability could have caused inaccuracies that are not accounted for in the credibility intervals, as the model assumes constant flow parameters and a constant magnetic field throughout the measurements.

Channel center-line measurements

LIF excitation schemes comparison

The final part of the experimental campaign was dedicated to the analysis of our LIF system capabilities. This consisted of making Kr I LIF measurements on multiple axial channel points to witness the evolution of the main neutral Krypton parameters. Here, all three transitions presented in "Lineshape modeling" section are used, to compare the precision resulting in fit parameters.

Some discrepancies are noticeable on T, but this could be due to slight variations in thruster operation points (see Fig. 9). The Hall thruster we used is a laboratory model, not optimized for long stationary operations. Since the measurements for the different transitions were taken on different days, it's possible that the thruster behaved slightly differently each time.

When comparing the precision of the different fits for the various transitions, the least precise inferences were associated with the 830.04 nm transition. This can be attributed to the smaller Landé factors g_j and SNR for this transition. On the other hand, the precision for the 826.55 nm and 828.33 nm transitions were similar. As expected, we witnessed a higher SNR for the 826.55 nm transition since, both for the 826.55 nm and 828.33 nm transitions, the lower level is $5s'[1/2]_1$, but the first resonance has double the probability of occurring. However, the Landé factors are larger for the 828 nm transition (see Table 1). As a result, these two effects offset each other.

For all three resonances, the inferred values of magnetic field intensity B and neutrals' drift velocity v_N are in strong agreement. Small discrepancies in B may be due to the self-induced magnetic fields, small deformations of the magnetic circuit caused by temperature gradients, or even deriving from the assumptions made on G and l (see "Lineshape modeling" section). In this last case, the fit procedure would introduce small unequal inaccuracies for different transitions.

The only variable recovered from the measurements with good precision in every location was v_N. On the contrary, T, θ^* and B show strong correlations between themselves at low B values (less than 100 G) reducing the fit capabilities with all the three LIF schemes (See Fig. 10). This results from the small Zeeman Effect experienced at those magnetic field intensities, not able to significantly alter the spectra. At the same time, the double polarization fit strategy shown in "Lineshape modeling" section substantially reduces this correlation, helping in having smaller credibility intervals for the various parameters.

With intermediate fields ($B > 100$ G), the fit strategy proved its capabilities, almost completely removing the correlation between B and the other parameters. A small

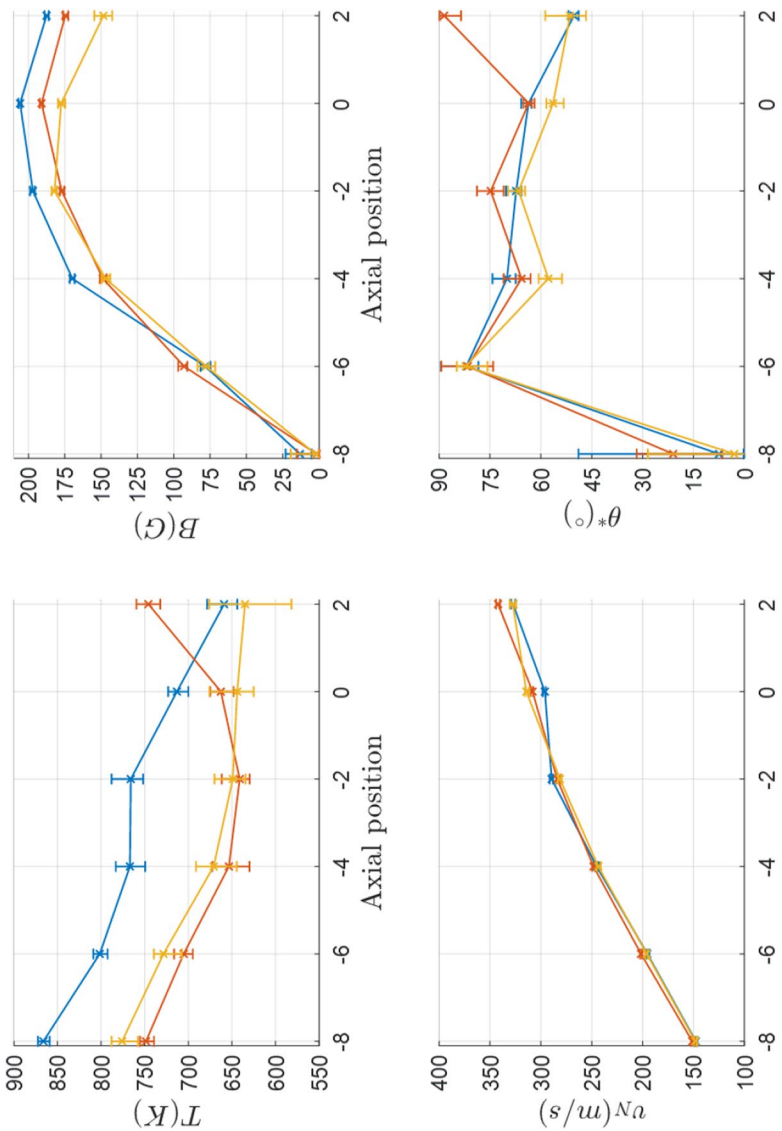

Fig. 9 Results of the channel center-line measurements campaign. The most probable value and 68% credibility intervals are shown for the four fit model variables of interest as a function of the axial position (the channel exit plane corresponds to 0 mm). The blue, orange and yellow lines are respectively for the inferred values using 826.55 nm, 828.33 nm and 830.04 nm transitions

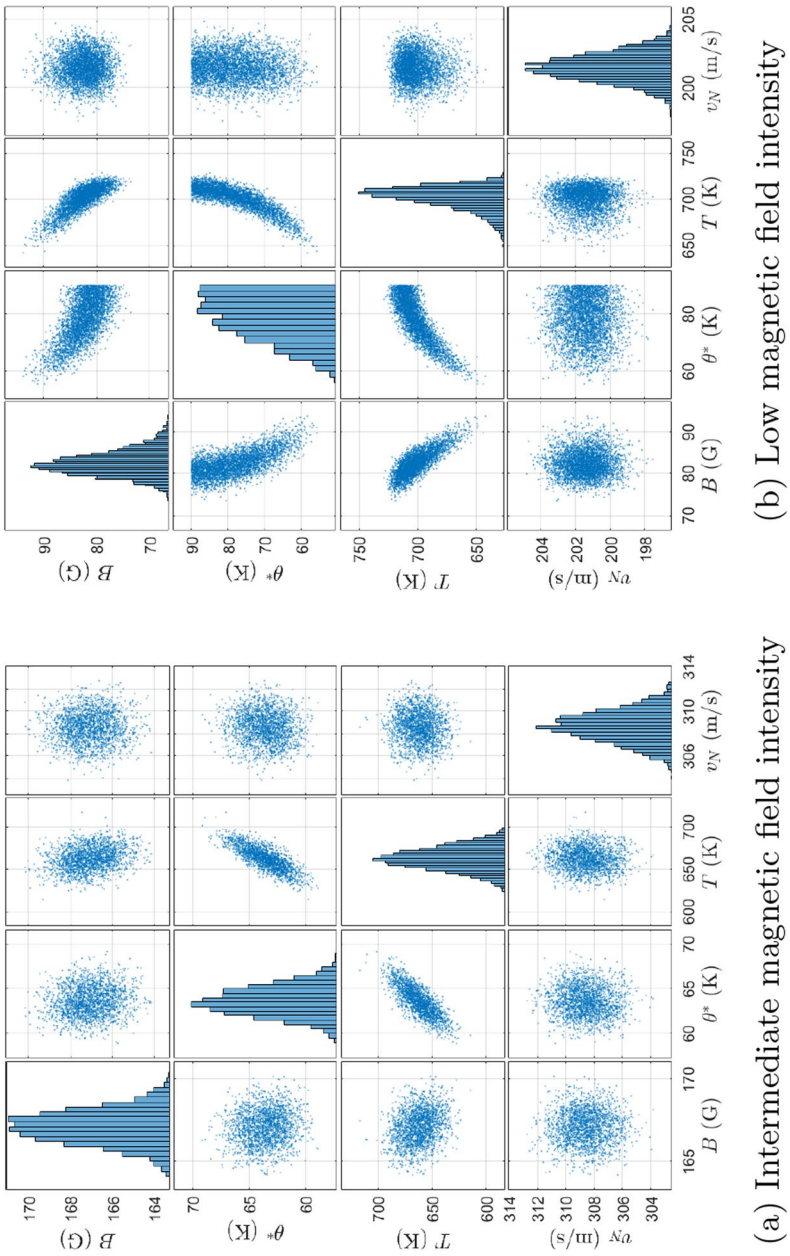

Fig. 10 Representative example of parameters correlation for low and intermediate magnetic field intensities

correlation between θ^* and T persists, also linked to a slight ellipticity in the fit that could not be eliminated by our experimental setup.

In any case, further analysis of the required SNR in different magnetic field configurations will be done, to determine an estimation of the measurement time needed to satisfy a possible requirement in the precision of the fit.

Considerations on Kr I measurements and prospective

A preliminary analysis of the results of the campaign was made to witness the phenomena happening in the thruster. A similar atomic flow drift velocity trend was already observed and discussed in Ref. [15, 17, 18]. It was shown that the effects that can lead to such acceleration of the neutrals could derive from two main causes:

- stronger depletion mechanisms resulting from ionization process of slow neutrals w.r.t. fast neutrals due to slow neutrals' longer residence times. Hence, they will likely experience more collisions that lead to ionization while crossing the thruster channel. The overall effect modifies the neutrals' VDF by shifting it toward the higher velocities;
- the presence of charge-exchange collisions. Therefore, fast ions, that experienced an acceleration due to the electric field in the thruster, may neutralize, increasing the fast neutrals' population. If these collisions happen at the beginning of the acceleration region, the ion velocities may still be comparable to the neutrals' velocities. Hence, the distribution function will not deviate much from an MB distribution but will be shifted toward faster speeds. Of course, after the acceleration region, the two velocities have a different order of magnitude, resulting in a deformation of the VDF;

Regarding the trend in T, we notice a small reduction toward the channel exit. We expect this to be due to a small expansion of the flow. This can also be caused by the first of the two aforementioned mechanisms leading to an apparent neutral acceleration. By partially removing the slow atoms from the neutrals' VDF, together with a shift of the mean velocity toward higher values, compression of the VDF may occur. This would lead to an apparent temperature reduction.

Further analysis of the small discrepancies in the magnetic field measurements will be done in the following campaigns. A better control of the laser polarization could significantly improve the fitting capabilities, making it possible to completely ignore the factors in Eq. 3 that account for the unknown ellipticity. Moreover, it is under development a system to polarize circularly the laser beam inside the vacuum chamber. In this way Eq. 3 would extremely simplify. For right-handed circular polarized light:

$$I_\pi = \sin(\theta)^2/2 \;\; I_{\sigma^\pm} = [(1 \pm \cos(\theta))/2]^2 \tag{9}$$

Hence, the dependence on ϕ would ideally disappear, and these measurements could substantially increase the accuracy on θ.

Further considerations must be made regarding anisotropies in fluorescence, as they could lead to inaccuracies in the geometric angles of the magnetic field.

Other transitions will be analyzed. Two other Kr I transitions seem promising, at about 810 nm and 811 nm. They share a metastable lower level. Therefore, we expect a

bigger population, hence a stronger signal-to-noise ratio. Analyzing different transitions from different lower states could even furnish information on the collision processes between electrons and neutrals, representing the main exciting mechanism. A calibration in intensity of the fluorescence collection system would be required, but this could be useful in combination with other diagnostic systems [6, 33], or even help in validating collisional-radiative models of the plasma [34, 35].

Application of time-resolved LIF techniques on neutrals could give a better picture of plasma instabilities. In particular, it would increase our capabilities in the identification of oscillations in the ionization region, one of the main phenomena related to breathing modes.

Finally, in thrusters presenting strong static magnetic fields, such as magnetic shielded HET and highly efficient multistage plasma thruster (HEMPT), or self-induced ones like MPD thrusters, non-intrusive spatially resolved measurements of the magnetic field could be crucial for reconstructing the ion VDF from ion LIF spectra [20] or retrieve essential information of the current densities in the device. In situations where there is prior knowledge of the magnetic field topology, strict priors can be applied to the magnetic field vector. This approach significantly improves the reconstruction of flow parameters. Consequently, the proposed measurement strategy can be easily tailored to meet different requirements by adjusting the prior information used in the Bayesian analysis.

Conclusions

Laser-induced fluorescence spectroscopy was utilized to investigate the neutral population within a laboratory model Hall thruster. A LIF spectra simulator was defined, comprehensive of various factors such as the natural mixture of the gas, the Doppler Effect, and the anomalous Zeeman Effect. An analysis of the Zeeman interaction with intermediate-to-low magnetic fields was developed, devoid of specific geometric assumptions.

Spectra originating from two different Kr I electronic states, namely $5s'[1/2]_1$ and $5s[3/2]_1$, are modelled, gathered and analyzed along the thruster center-line, until the channel exit. An examination of the differences in the derived parameters arising from the utilization of different transitions, as well as their spatial evolution, was conducted.

A new robust and flexible data elaboration strategy for neutrals' LIF spectra based on laser polarization is presented. The spectra with two orthogonal polarizations are acquired, reducing the correlation between neutrals' temperature and magnetic field. Analysis of data fit residuals together with an experimental campaign focused on the inference of the magnetic field have been made, validating both the model and the strategy here defined. Bayesian approach was exploited to increase data elaboration capabilities.

Finally, a background on possible future applications and further improvements on the technique are given, based on the weaknesses and strengths of our apparatus understood during the experimental campaign.

Acknowledgements

M.D.V. acknowledges the financial support of the University of Siena and of Toscana Region through AdR6 2023 - Project DIPE , CUP: B63C23000490002.

Authors' contributions

M.D.V. leading role in the conceptualization of the work, development of the theoretical model, designing and performing the experiment including its validation with the theoretical model, and writing of the manuscript. Y.D. contributed to the conceptualization of the work, leading role in designing and performing the experiment. A.K. and P.C. contributed

to the development of the experimental setup. E.M. contributed to the conceptualization of the work. F.S. contributed to the conceptualization of the work and funding acquisition. All the authors contributed to the reviewing of the manuscript.

Funding
No funding was received for conducting this study.

Data availability
No datasets were generated or analysed during the current study.

Declarations

Competing interests
The authors declare no competing interests.

Received: 19 November 2024 Accepted: 25 March 2025
Published online: 11 April 2025

References

1. Goebel DM, Katz I (2008) Fundamentals of electric propulsion : ion and Hall thrusters. JPL space science and technology series; 1. Wiley, Hoboken. https://doi.org/10.1002/9780470436448
2. Mazouffre S (2016) Electric propulsion for satellites and spacecraft: established technologies and novel approaches. Plasma Sources Sci Technol 25(3):033002. https://doi.org/10.1088/0963-0252/25/3/033002
3. Giammarinaro G, Marconcini F, Becatti G, Saravia MM, Andrenucci M, Paganucci F (2023) A scaling methodology for high-power magnetically shielded Hall thrusters. J Electr Propuls 2(1):17. https://doi.org/10.1007/s44205-023-00049-8
4. Battista F, De Marco E, Misuri T, Andrenucci M (2007) A review of the Hall thruster scaling methodology. 30th International Electric Propulsion Conference, Firenze September 17-20, Italy. IEPC-2007-313
5. Boeuf JP (2017) Tutorial: Physics and modeling of hall thrusters. J Appl Phys 121(1):011101. https://doi.org/10.1063/1.4972269
6. Roberts PJ, Jorns BA (2024) Laser measurement of anomalous electron diffusion in a crossed-field plasma. Phys Rev Lett 132:135301. https://doi.org/10.1103/PhysRevLett.132.135301
7. Dancheva Y, Pagano D, Scaranzin S, Mercatelli R, Presi M, Scortecci F, Castellini G (2022) Non-intrusive tools for electric propulsion diagnostics. CEAS Space J 14(1):19–30. https://doi.org/10.1007/s12567-021-00360-w
8. Mullins CR, Farnell CC, Farnell CC, Martinez RA, Liu D, Branam RD, Williams JD (2017) Non-invasive Hall current distribution measurement in a Hall effect thruster. Rev Sci Instrum 88(1):013507. https://doi.org/10.1063/1.4974098
9. Morishita T, Tsukizaki R, Nishiyama K, Kuninaka H (2022) Plasma parameters measured inside and outside a microwave-discharge-based plasma cathode using laser-induced fluorescence spectroscopy. J Appl Phys 131(1):013301. https://doi.org/10.1063/5.0071294
10. Pérez-Luna J, Hagelaar GJM, Garrigues L, Boeuf JP (2009) Method to obtain the electric field and the ionization frequency from laser induced fluorescence measurements. Plasma Sources Sci Technol 18(3):034008. https://doi.org/10.1088/0963-0252/18/3/034008
11. Vaudolon J, Balika L, Mazouffre S (2013) Photon counting technique applied to time-resolved laser-induced fluorescence measurements on a stabilized discharge. Rev Sci Instrum 84(7):073512. https://doi.org/10.1063/1.4816642
12. Dancheva Y, Coniglio P, Da Valle M, Scortecci F (2023) Ion dynamic characterization using phase-resolved laser-induced fluorescence spectroscopy in a Hall effect thruster. Rev Sci Instrum 94(7):073503. https://doi.org/10.1063/5.0146669
13. Chaplin VH, Lobbia RB, Lopez Ortega A, Mikellides IG, Hofer RR, Polk JE, Friss AJ (2020) Time-resolved ion velocity measurements in a high-power Hall thruster using laser-induced fluorescence with transfer function averaging. Appl Phys Lett 116(23):234107. https://doi.org/10.1063/5.0007161
14. Vaudolon J, Khiar B, Mazouffre S (2014) Time evolution of the electric field in a Hall thruster. Plasma Sources Sci Technol 23(2):022002. https://doi.org/10.1088/0963-0252/23/2/022002
15. Ngom BB, Smith TB, Huang W, Gallimore AD (2008) Numerical simulation of the Zeeman effect in neutral Xenon from NIR diode-laser spectroscopy. J Appl Phys 104(2):023303. https://doi.org/10.1063/1.2955761
16. Huang W, Ngom BB, Gallimore AD (2009) Using nonlinear Zeeman spectroscopy to obtain in-situ magnetic field measurement in a Hall thruster. 31st International Electric Propulsion Conference. Michigan September 20-24, USA. IEPC-2009-088
17. Mazouffre S, Bourgeois G, Garrigues L, Pawelec E (2011) A comprehensive study on the atom flow in the cross-field discharge of a Hall thruster. J Phys D Appl Phys 44(10):105203. https://doi.org/10.1088/0022-3727/44/10/105203
18. Vinci AE, Mazouffre S, Gómez V, Fajardo P, Navarro-Cavallé J (2022) Laser-induced fluorescence spectroscopy on Xenon atoms and ions in the magnetic nozzle of a helicon plasma thruster. Plasma Sources Sci Technol 31(9):095007. https://doi.org/10.1088/1361-6595/ac8db8
19. Knigge A, Schulz M, Knothe C, Oechsner U (2021) Polarization analyzer for fiber optics and free beam applications. PhotonicsViews 18(3):74–78. https://doi.org/10.1002/phvs.202100042
20. Dancheva Y, Funalbi S, Coniglio P, Garde A, Pagano D, Scortecci F, Lazurenko A, Weis S, Genovese A, Holtmann P, Da Valle M, Biancalana V, Mariotti E (2025) Laser-induced fluorescence spectroscopy for Kr thrusters. J Electr Propuls 4(1):12. https://doi.org/10.1007/s44205-025-00111-7

21. Sobelman II (1992) Atomic spectra and radiative transitions. Springer Series on Atoms and Plasmas, Springer, Heidelberg. https://doi.org/10.1007/978-3-642-76907-8
22. Pietzonka L, Eichhorn C, Scholze F, Spemann D (2023) Laser-induced fluorescence spectroscopy for kinetic temperature measurement of xenon neutrals and ions in the discharge chamber of a radiofrequency ion source. J Electr Propuls 2(1):4. https://doi.org/10.1007/s44205-022-00029-4
23. Sackers M, Marchuk O, Dipti D, Ralchenko Y, Ertmer S, Brezinsek S, Kreter A (2024) Zeeman effect of isotopes of Kr and Xe investigated at the linear plasma device PSI-2. Plasma Sources Sci Technol 33(2):025015. https://doi.org/10.1088/1361-6595/ad23fa
24. Tremblay P, Michaud A, Levesque M, Thériault S, Breton M, Beaubien J, Cyr N (1990) Absorption profiles of alkali-metal D lines in the presence of a static magnetic field. Phys Rev A 42:2766–2773. https://doi.org/10.1103/PhysRevA.42.2766
25. Hagelaar GJM, Pitchford LC (2005) Solving the Boltzmann equation to obtain electron transport coefficients and rate coefficients for fluid models. Plasma Sources Sci Technol 14(4):722. https://doi.org/10.1088/0963-0252/14/4/011
26. Kaufman V (1993) Wavelengths and Energy Levels of Neutral Kr(84) and Level Shifts in All Kr Even Isotopes. J Res Natl Inst Stand Technol 98(6):717–724. https://doi.org/10.6028/jres.098.047
27. Saloman EB (2007) Energy Levels and Observed Spectral Lines of Krypton, Kr I through Kr XXXVI. J Phys Chem Ref Data 36(1):215–386. https://doi.org/10.1063/1.2227036
28. Feroz F, Hobson MP, Bridges M (2009) MultiNest: an efficient and robust Bayesian inference tool for cosmology and particle physics. Mon Not R Astron Soc 398(4):1601–1614. https://doi.org/10.1111/j.1365-2966.2009.14548.x
29. Veitch J, Vecchio A (2010) Bayesian coherent analysis of in-spiral gravitational wave signals with a detector network. Phys Rev D 81(6). https://doi.org/10.1103/physrevd.81.062003
30. Saravia MM, Giacobbe A, Andreussi T (2019) Bayesian analysis of triple Langmuir probe measurements for the characterization of Hall thruster plasmas. Rev Sci Instrum 90(2):023502. https://doi.org/10.1063/1.5079532
31. Giannetti V, Saravia MM, Andreussi T (2020) Measurement of the breathing mode oscillations in Hall thruster plasmas with a fast-diving triple Langmuir probe. Phys Plasmas 27(12):123502. https://doi.org/10.1063/5.0022928
32. Peterson PY, Gallimore AD, Haas JM (2002) An experimental investigation of the internal magnetic field topography of an operating Hall thruster. Phys Plasmas 9(10):4354–4362. https://doi.org/10.1063/1.1507771
33. Han L, Gao J, Chen T, Cong Y, Li Z (2019) A method to measure the in situ magnetic field in a hall thruster based on the Faraday rotation effect. Plasma Sci Technol 21(8):085502. https://doi.org/10.1088/2058-6272/ab0f63
34. Wang YF, Zhu XM (2019) A comprehensive xenon collisional-radiative model of atomic and ionic excited levels for Hall thruster. 36th International Electric Propulsion Conference, Vienna September 15-20, Austria. IEPC-2019-306
35. Zhu XM, Wang YF, Wang Y, Yu DR, Zatsarinny O, Bartschat K, Tsankov TV, Czarnetzki U (2019) A xenon collisional-radiative model applicable to electric propulsion devices: II. Kinetics of the 6s, 6p, and 5d states of atoms and ions in Hall thrusters. Plasma Sources Sci Technol 28(10):105005. https://doi.org/10.1088/1361-6595/ab30b7

Publisher's Note